JOURNAL OF SOLID STATE CHEMISTRY 116, 179–184 (1995)

Phase Transformation in $Pb_4(PO_4)_2CrO_4$

Jacques Barbier[1] and David Maxin

Department of Chemistry, McMaster University, Hamilton, Ontario L8S 4M1, Canada

Received June 8, 1994; in revised form October 11, 1994; accepted October 13, 1994

A phase transformation has been discovered in the $Pb_4(PO_4)_2CrO_4$ compound between a high-temperature cubic eulytite-type phase and a low-temperature rhombohedral $Pb_3(PO_4)_2$-type phase. Structural refinements of both phases have been carried out using neutron powder diffraction data. The possible role in the transformation of the stereoactive lone-pairs of electrons on the Pb atoms is discussed.

1. INTRODUCTION

The two Pb compounds, $Pb_4(PO_4)_2SO_4$ and $Pb_4(PO_4)_2CrO_4$, were originally characterized by powder X-ray diffraction as belonging to the eulytite, $Bi_4(SiO_4)_3$, structural family (1). As part of an on-going study of the crystal chemistry of the eulytite structure type, the structure of $Pb_4(PO_4)_2SO_4$ has recently been refined using both X-ray single-crystal and neutron powder data (2, 7, 8). A concomitant powder diffraction study of the analogous $Pb_4(PO_4)_2CrO_4$ revealed the existence of a phase transformation at around 700°C between a high-temperature eulytite form and a low-temperature form corresponding to a Pb-deficient $Pb_3(PO_4)_2$ structure. A similar transformation, albeit occurring at much higher temperatures around 1200–1400°C, had previously been observed but not investigated in detail in the case of $Sr_4(PO_4)_2CrO_4$ (3). In order to obtain insights into the crystal chemistry of this transformation, structure refinements by powder neutron diffraction of both low- and high-temperature forms of $Pb_4(PO_4)_2CrO_4$ have been undertaken, the results of which are presented in this paper.

2. EXPERIMENTAL

Powder samples of $Pb_4(PO_4)_2CrO_4$ were prepared from stoichiometric mixtures of $(PbCO_3)_2Pb(OH)_2$, $(NH_4)_2CrO_4$, and $NH_4H_2PO_4$ powders of analytical grade purity. The possibility of a phase transformation was initially revealed by the different colors of samples synthesized at temperatures of 500°C (green-yellow) and 800°C (orange). The structural nature of this transformation was confirmed by a DTA experiment showing a sharp endothermic peak at 710°C upon heating (at a rate of 10°C/min) and by recording X-ray powder patterns (Guinier–Hägg camera) of the low-temperature phase and the (quenched) high-temperature phase. Although no sign of reversibility could be observed on the DTA cooling curve, this was later determined to be due to the sluggishness of the reverse transformation which required annealing for 3–4 days at 500°C to yield a pure low-temperature phase. The X-ray powder pattern of the high-temperature phase was readily indexed on a cubic eulytite-type unit-cell ($I\bar{4}3d$ space group, a = 10.5390(1) Å) similar to that reported originally (1). The pattern of the low-temperature phase was indexed with the help of an indexing program (4) on a rhombohedral unit-cell (a = 5.5403(1) Å, c = 20.4999(4) Å) similar to that of the high-temperature form of $Pb_3(PO_4)_2$ (5).

For the neutron diffraction experiments, a large powder sample (about 8 g) of $Pb_4(PO_4)_2CrO_4$ was synthesized from the same starting materials as described above. In a first stage, the low-temperature form was prepared by heating the sample in steps up to 650°C, keeping it at that temperature for 5 days, and finally quenching it in air. In a second stage, after the collection of the diffraction data for the low-temperature form, the high-temperature form was obtained by heating the same sample at 800°C for 4 days and quenching it in air. The neutron powder diffraction experiments were carried out at room-temperature using a 1.3913 Å neutron beam from a (200) copper monochromator at the McMaster Nuclear Reactor. The samples were contained in a thin-walled vanadium can and the data were collected in steps of 0.1° (2θ) over angular ranges of $10 < 2\theta < 100°$ (low-T form) and $15 < 2\theta < 105°$ (high-T form) at four successive settings of the position-sensitive detector. After correction of the raw data for detector geometry, the Rietveld profile refinements were carried out with the PC version of the DBWS software (6).

3. REFINEMENT OF CUBIC $Pb_4(PO_4)_2CrO_4$

The starting model for the refinement of the high-temperature form of $Pb_4(PO_4)_2CrO_4$ was based on the struc-

[1] To whom correspondence should be addressed.

0022-4596/95 $6.00

ture of eulytite-type $Pb_4(PO_4)_2SO_4$ (2): in the $I\bar{4}3d$ space group, the Pb atoms occupy the 16*c* positions on the threefold axes of the unit cell, the P and Cr atoms are disordered on the 12*a* positions with $\bar{4}$ symmetry and the oxygen atoms are split over two partially filled 48*e* general positions. This oxygen disorder contributes to the high background visible in the neutron powder pattern (cf. Fig. 1a) and has also been observed in other phosphate eulytites of the type $A_3B(PO_4)_3$ (7, 8). A total of 22 parameters were allowed to vary during the Rietveld refinement including profile parameters (scale factor, background polynomial, linewidth parameters for the Gaussian lineshape, zero point, sample displacement, and peak asymmetry) and structural parameters (unit-cell parameter, atomic coordinates, isotropic temperature factors, and populations of the O1 and O2 oxygen sites). No significant preferred orientation was detected, and attempts at refining anisotropic temperature factors did not yield any significant improvement and led to nonpositive values for the oxygen atoms. After convergence, the following agreement indices were obtained: weighted profile $R_{w_p} = 0.060$, Bragg $R_B = 0.067$, expected $R_e = 0.027$, goodness-of-fit $S = 2.18$, and weighted Durbin–Watson statistic $D = 0.47$. The final plots of observed and calculated intensity profiles and their difference are shown in Fig. 1a. The corresponding atomic coordinates, isotropic temperature factors and selected bond lengths and angles are listed in Table 1. It should be noted here that the previous determination of the $Pb_4(PO_4)_2SO_4$ eulytite

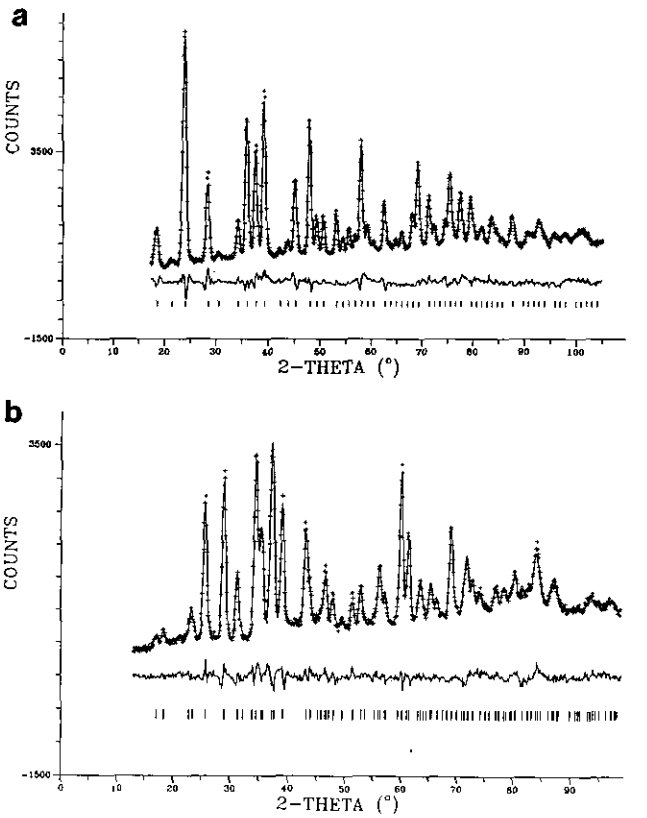

FIG. 1. Profiles of observed and calculated powder neutron intensities for $Pb_4(PO_4)_2CrO_4$ in the high-temperature cubic eulytite-type form (a) and in the low-temperature rhombohedral $Pb_3(PO_4)_2$-type form (b). Note the high backgrounds in both cases and the lower signal/noise ratio in (b).

TABLE 1

Atomic Coordinates, Isotropic Temperature Factors, and Bonding Geometry for the High-Temperature Form of $Pb_4(PO_4)_2CrO_4$ ($I\bar{4}3d$, $a = 10.5390(1)$ Å, $Z = 4$)

Atom	Site	*x*	*y*	*z*	*B* (Å²)
Pb	16c	0.0729(2)	0.0729(2)	0.0729(2)	1.71(8)
P, Cr	12a	0.375	0.0	0.25	0.7(2)
O1[a]	48e	0.5697(8)	0.3548(8)	0.7080(10)	1.8(1)
O2[a]	48e	0.5347(9)	0.3675(9)	0.7092(9)	1.8(1)

Bond lengths (Å) and angles (°)

Pb–O1	2.432(10) × 3	(P, Cr)–O1	1.589(9) × 4
	2.704(9) × 3		
	[3.276(9) × 3]	O1–(P, Cr)–O1	107.6(4) × 4
			113.2(5) × 2
O1–Pb–O1	73.7–116.3		
Pb–O2	2.415(10) × 3	(P, Cr)–O2	1.567(9) × 4
	2.629(10) × 3		
	[3.656(10) × 3]	O2–(P, Cr)–O2	108.7(5) × 4
			111.0(5) × 2
O2–Pb–O2	70.7–114.0		

Note. Esd's are given in brackets.

[a] The O1 and O2 sites are half-filled only with refined populations of 50(1)% each. Their temperature factors were constrained to be equal.

structure from single-crystal X-ray and powder neutron data (2) showed that the structure was best described in the cubic $I\bar{4}3d$ space group with P/S disorder. Therefore, the same model was used in the present work and no attempt has been made to resolve the P/Cr disorder by, for instance, carrying out the refinement in a lower-symmetry space group such as $I\bar{4}2d$, a tetragonal subgroup of $I\bar{4}3d$.

The eulytite structure of high-T $Pb_4(PO_4)_2CrO_4$ viewed along the [111] direction is shown in Fig. 2a. It consists of a three-dimensional framework of edge-shared PbO_6 octahedra also sharing corners with (P, Cr)O_4 tetrahedra. An alternative description of the structure, originally applied to the structure of the eulytite mineral $Bi_4(SiO_4)_3$ (9), emphasizes the packing of Pb_8 bisdisphenoids centered by (P, Cr)O_4 tetrahedra. In this case, the oxygen disorder associated with the partial occupancies of the O1 and O2 positions has been shown to correspond to a rotation of the (P, Cr)O_4 tetrahedra around their $\bar{4}$ axis (cf. Fig. 1 in Ref. (2)). The bond length and angle data in Table 1 show that the tetrahedra are fairly regular for both the O1 and O2 sites, with bond lengths in agreement

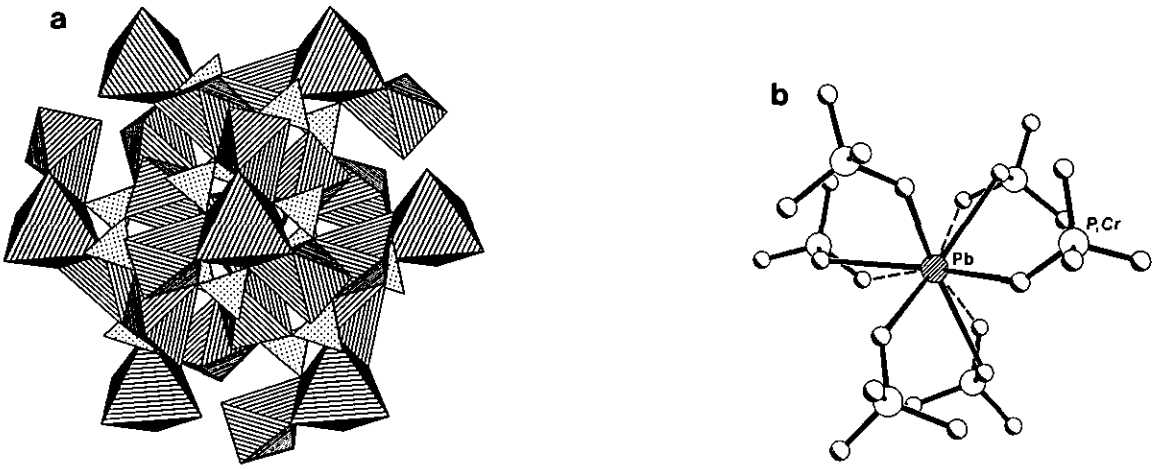

FIG. 2. (a) View of the eulytite-type $Pb_4(PO_4)_2CrO_4$ structure along the [111] direction showing the framework of edge-sharing PbO_6 octahedra and corner-sharing (P, Cr)O_4 tetrahedra. (b) Coordination environment of the Pb atoms in cubic $Pb_4(PO_4)_2CrO_4$ viewed along the [111] direction. The stereoactive lone-pair of electrons on the Pb atom distorts the PbO_6 octahedron and, pointing in the plane of the figure, also yields three more essentially nonbonding Pb–O distances of over 3.25 Å (dashed lines). The figure has been drawn using the O1 oxygen position (cf. Table 1).

with the expected values for the PO_4^{3-} and CrO_4^{2-} tetrahedral anions (1.55 and 1.64 Å, respectively (10)). The coordination of the Pb atoms is illustrated in Fig. 2b (for the O1 position): it corresponds to a strongly distorted octahedron (cf. Table 1), compressed along its threefold axis, with three short and three long bonds and with next-nearest oxygen neighbors at distances of more than 3.2 Å (represented by dashed lines in Fig. 2b). This type of distortion is typical of lone-pair cations such as Pb^{2+} and Bi^{3+} and appears to be required by the topology of the eulytite structure. (It is, for instance, not possible to build a model of the structure with regular octahedra and tetrahedra.) In spite of these distortions, bond valence sums (11) around the Pb atoms lead to normal values of 2.00 for the O1 position (including the three Pb–O1 bonds at 3.276 Å) and 2.06 for the O2 position (without including the three Pb–O2 distances at 3.656 Å which have a bond valence of only 0.01 each).

4. REFINEMENT OF RHOMBOHEDRAL $Pb_4(PO_4)_2CrO_4$

As mentioned above, the X-ray powder pattern of the low-temperature form of $Pb_4(PO_4)_2CrO_4$ suggested that it could be isostructural with rhombohedral $Pb_3(PO_4)_2$ as had been reported earlier in the case of $Sr_4(PO_4)_2CrO_4$ (3). However, the different stoichiometry implies a Pb deficiency in $Pb_4(PO_4)_2CrO_4$ which leads to the following atomic distributions in the two compounds (positions in the $R\bar{3}m$ space group): for $Pb_3(PO_4)_2$, $Z = 3$, Pb1, Pb2, O1, and O2 occupy the $3a$, $6c$ (×3), and $18h$ sites, respectively; for $Pb_4(PO_4)_2CrO_4$, $Z = 2$, Pb1, Pb2, (P, Cr), O1, and O2 occupy the $3a$, $6c$ (×3), and $18h$ sites, respectively, with partial occupancies of the Pb sites to yield eight Pb atoms per unit cell.

The starting model for the Rietveld refinement of low-T $Pb_4(PO_4)_2CrO_4$ was therefore based on the rhombohedral $Pb_3(PO_4)_2$ (5) structure with deficient Pb sites and disordered P and Cr atoms on the tetrahedral sites. As shown in Fig. 1, the background was much more prominent in the neutron powder pattern of the rhombohedral phase than in that of the cubic phase, and this led to an unsatisfactory refinement of the background polynomial function which was therefore replaced by linear interpolations over 12 segments along the pattern. Initial cycles of refinement quickly indicated that the Pb vacancies were concentrated on the Pb2 site and the refinement was carried on with fixed occupancies of 1 and 5/6 for the Pb1 and Pb2 sites, respectively. In the final cycles of the refinement, a total of 23 parameters were allowed to vary including profile parameters (scale factor, zero point, sample displacement, linewidth of the Gaussian lineshape, and peak asymmetry) and structural parameters (unit-cell parameters, atomic coordinates, and anisotropic temperature factors for all atoms). A parameter for a possible (001) preferred orientation was also refined but did not deviate significantly from the value expected for a randomly oriented powder. After convergence, the following agreement indices were obtained: weighted profile $R_{w_p} = 0.049$, Bragg $R_B = 0.068$, expected $R_e = 0.029$, goodness-of-fit $S = 1.66$, and weighted Durbin–Watson statistic $D = 0.80$. The final plots of observed and calculated intensity profiles and their difference are shown in Fig. 1b. The corresponding atomic coordinates, temperature factors, and selected bond lengths and angles are listed in Table 2. These data show abnormally large temperature factors for the Pb1, Pb2, and O1 atoms, as well as a strong anisotropy in the hexagonal basal plane for all the atoms. This suggests that the refined atomic positions

TABLE 2

Atomic Coordinates, Temperature Factors, and Bonding Geometry for the Low-Temperature Form of $Pb_4(PO_4)_2CrO_4$ ($R\bar{3}m$, a = 5.5403(1) Å, c = 20.4999(4) Å, Z = 2)

Atom	Site	x	y	z	B_{eq} (Å^2)[a]
Pb1	3*a*	0.0	0.0	0.0	2.84
Pb2[b]	6*c*	0.0	0.0	0.2071(3)	6.16
P, Cr	6*c*	0.0	0.0	0.4037(4)	1.82
O1	6*c*	0.0	0.0	0.3274(3)	4.34
O2	18*h*	0.1805(6)	0.3610(6)	0.0961(2)	1.89

Atom	β_{11}	β_{22}	β_{33}	β_{12}	β_{13}	β_{23}
Pb1	0.047(4)	0.047(4)	0.0023(3)	0.024(4)	0.0	0.0
Pb2[b]	0.092(4)	0.092(4)	0.0009(2)	0.046(4)	0.0	0.0
P, Cr	0.016(4)	0.016(4)	0.0015(3)	0.008(4)	0.0	0.0
O1	0.057(4)	0.057(4)	0.0015(3)	0.028(4)	0.0	0.0
O2	0.017(2)	0.012(2)	0.0017(2)	0.006(2)	−0.0008(4)	−0.0016(4)

Bond lengths (Å) and angles (°)

Pb1–O1	3.201(1) × 6	(P, Cr)–O1	1.564(12)
–O2	2.623(6) × 6	–O2	1.559(6) × 3
Pb2–O1	2.466(9)	O1–(P, Cr)–O2	109.8(4) × 3
–O2	2.841(5) × 6	O2–(P, Cr)–O2	109.2(4) × 3
–O2	2.860(7) × 3		

Note. Esd's are given in brackets.

[a] $B_{eq} = 4/3 \sum_i \sum_j \beta_{ij} \mathbf{a}_i \cdot \mathbf{a}_j$.

[b] The Pb2 site has a partial occupancy of 5/6.

correspond to an average structure only which, indeed, is consistent with the observation by electron diffraction of a very weak (2 × **a**) superstructure. However, no superstructure reflections could be detected in the X-ray or neutron powder patterns, and attempts to refine the structure on a larger unit cell were unsuccessful. It is interesting to note that an even larger (2 × **a**, 2 × **c**) cell has been reported for the analogous low-temperature form of $Sr_4(PO_4)_2CrO_4$ (3). In both compounds, the formation of a superstructure could be related to some ordering of the metal vacancies on the *M*2 sites located within layers perpendicular to the *c*-axis.

The coordination geometry in the low-T $Pb_4(PO_4)_2CrO_4$ structure is illustrated in Fig. 3a showing the linear linkage parallel to the [001] direction of tetrahedra and PbO_n polyhedra. On one hand, the (P, Cr)O_4 tetrahedron is quasi-regular with a bond length similar to that in the high-T eulytite phase. On the other hand, the two Pb environments are rather irregular and quite different from each other (cf. Table 2): Pb1 is located on a center of symmetry and is bonded to 12 oxygens forming a distorted cuboctahedron with six Pb1–O2 bonds of 2.62 Å and six much longer equatorial Pb1–O1 bonds of 3.20 Å; Pb2 has a less symmetric environment of 10 oxygens with, in particular, one short Pb2–O1 bond of 2.47 Å. These coordination polyhedra are characteristic of this structure type and are also encountered in the isostruc-

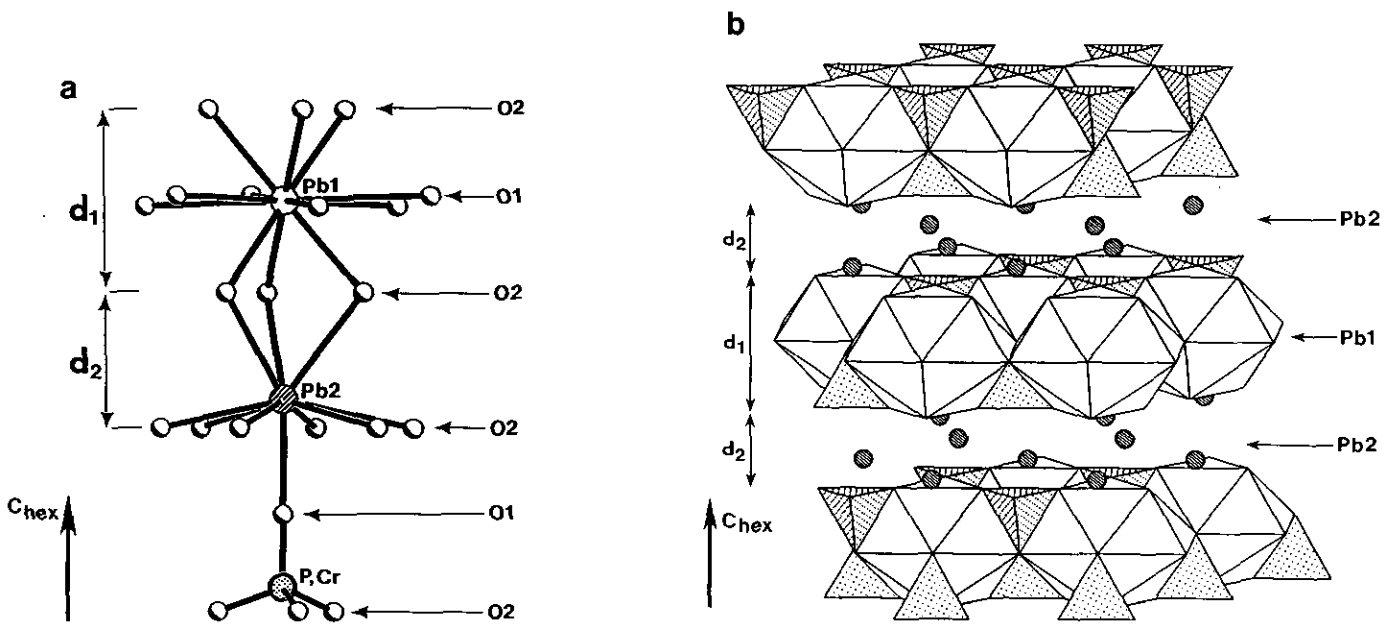

FIG. 3. (a) Coordination environments in rhombohedral $Pb_4(PO_4)_2CrO_4$ showing the linkage of polyhedra (P, Cr)O_4–Pb2(O_{10})–Pb1(O_{12})–Pb2(O_{10})–(P, Cr)O_4... along the [001] direction. (b) Perspective view of the rhombohedral $Pb_4(PO_4)_2CrO_4$ structure emphasizing the layers formed by the Pb1(O_{12}) and (P, Cr)O_4 polyhedra and joined via the Pb2 atoms. The partial occupancy of the Pb2 sites leads to a smaller interlayer spacing (d_2) than in the isostructural $Pb_3(PO_4)_2$ compound (see text).

TABLE 3

Comparison of Cell Parameters and Layer Spacings in the Structures of Low-T $Pb_4(PO_4)_2CrO_4$, $Pb_3(PO_4)_2$ (5), and $Ba_3(PO_4)_2$ (13)

	Low-T $Pb_4(PO_4)_2CrO_4$	$Pb_3(PO_4)_2$	$Ba_3(PO_4)_2$
a (Å)	5.540	5.530	5.604
c (Å)	20.499	20.277	21.000
d_1 (Å)	3.94	3.79	4.16
d_2 (Å)	2.89	2.97	2.83

tural phosphates β-$Pb_3(PO_4)_2$ (5, 12) and (Sr, Ba)$_3(PO_4)_2$ (13) and the corresponding vanadates γ-$Pb_3(VO_4)_2$ (14) and $Sr_3(VO_4)_2$ (15). Bond valence sum calculations (11) yield values of 1.82 for Pb1 and 1.61 for Pb2, the latter being consistent with the partial occupancy of that site.

A polyhedral representation of the low-T $Pb_4(PO_4)_2CrO_4$ structure is shown in Fig. 3b, emphasizing its layer character. The layers are perpendicular to the c-axis and are built of edge-sharing Pb1(O_{12}) polyhedra and (P, Cr)O_4 tetrahedra. The Pb2 atoms are located between the layers but just above and below the planes defined by the O2 atoms (cf. Fig. 3a) so that the interlayer bonding is achieved through the three long Pb2–O2 bonds of 2.86 Å (cf. Table 2). The asymmetric coordination of the Pb2 atoms with a short Pb2–O1 bond on one side (within the layers) and three long Pb2–O2 bonds on the other (between the layers) is a result of the stereoactivity of the lone-pair of electrons associated with Pb^{2+} ions. This interpretation is clearly supported by the comparison of cell parameters and layer spacings (d_1 and d_2; cf. Fig. 3b) in the isostructural compounds low-T $Pb_4(PO_4)_2CrO_4$, β-$Pb_3(PO_4)_2$, and $Ba_3(PO_4)_2$ (Table 3). For instance, in spite of a shorter c-parameter in β-$Pb_3(PO_4)_2$, the d_2 interlayer spacing is actually slightly larger than in $Pb_4(PO_4)_2CrO_4$ (2.97 vs 2.89 Å), which is consistent with the full occupancy of the Pb2 site in the former compound resulting in stronger repulsive interactions due to the lone-pairs of adjacent layers. In contrast, the total absence of stereoactive lone-pairs in $Ba_3(PO_4)_2$ allows the layers to move closer together than in $Pb_4(PO_4)_2CrO_4$, yielding a smaller d_2 spacing of 2.83 Å, even though the c-axis is larger due to the larger Ba atoms.

5. THE RHOMBOHEDRAL ↔ CUBIC TRANSFORMATION IN $Pb_4(PO_4)_2CrO_4$

The compounds $Sr_4(PO_4)_2CrO_4$ (3) and $Pb_4(PO_4)_2CrO_4$ are apparently the only ones that have been reported to undergo a transformation between a low-temperature rhombohedral $Pb_3(PO_4)_2$-type structure and a high-temperature cubic eulytite-type structure. However, a significant difference between these two compounds lies in their transformation temperature, which is above 1200°C for the Sr case and only about 700°C for the Pb case. This large difference possibly reflects the presence of stereoactive lone-pairs of electrons in $Pb_4(PO_4)_2CrO_4$ which, as discussed below, might play a role in the transformation. In that respect, it should be noted that the stereoactivity of the Pb^{2+} lone-pairs has recently been shown to be an important factor in the transformations between the α, β, and γ forms of $Pb_3(VO_4)_2$ (14), the γ form being isostructural with rhombohedral $Pb_3(PO_4)_2$.

The major structural changes associated with the rhombohedral → cubic transformation in $Pb_4(PO_4)_2CrO_4$ are changes in the Pb coordination environments (cf. Tables 1 and 2), a change from a layer structure to a framework structure (cf. Figs. 3b and 2a), the elimination of Pb vacancies, and a volume increase of 7.4% per $Pb_4(PO_4)_2CrO_4$ formula unit. As described in the previous section, the layer character of the rhombohedral structure is caused by the stereoactive lone-pairs at the Pb2 sites which keep the layers apart and weaken the interlayer bonding. The stereoactivity of the lone-pairs is also present in the cubic structure which, in spite of a larger volume per Pb atom, contains strongly distorted PbO_6 octahedra with shorter average Pb–O bonds than the rhombohedral structure. However, all Pb atoms occupy equivalent positions on the threefold axes of the structure in such a manner that their lone-pairs do not interact significantly with one another: for adjacent Pb atoms in edge-shared octahedra they point along different ⟨111⟩ directions, and for Pb atoms on the same threefold axis they point the same way along that [111] direction (cf. Fig. 2a). This particular topology of the eulytite structure, together with its increased volume, allows it to better accommodate the electron density associated with the lone-pairs of the Pb atoms, and it may be argued that this is a driving force for the rhombohedral → cubic transformation taking place in $Pb_4(PO_4)_2CrO_4$ upon heating at about 700°C. Evidently, this is not the only driving force, since the same transformation takes place in $Sr_4(PO_4)_2CrO_4$ (3) where no lone-pairs are present. In this case, however, the eulytite structure becomes stable only at much higher temperatures as, has been previously observed for other phosphates of the type $MLn_3(PO_4)_3$ (M = Sr, Ba; Ln = trivalent rare earth) without lone-pair cations (8, 16). Consequently, the presence of stereoactive lone-pairs in $Pb_4(PO_4)_2CrO_4$ appears to be a destabilizing factor for the low-temperature rhombohedral phase as well as a stabilizing factor for the high-temperature cubic phase, thereby resulting in a sharp drop in the transformation temperature. From the viewpoint of the reverse transformation, the presence of oxygen disorder in the cubic structure (a feature apparently common to all eulytite compounds except the simple-type compounds $Bi_4(SiO_4)_3$ and $Bi_4(GeO_4)_3$ (2, 7, 8)) suggests that it is sta-

ble at high temperatures only and should, therefore, undergo some transformation at moderate-to-low temperatures. Indeed, decomposition reactions at temperatures below 1200°C have previously been reported for the $MLn_3(PO_4)_3$ phases (16), but the present transformation to a $Pb_3(PO_4)_2$-type structure is the only example of a polymorphic transformation for eulytite-type compounds.

ACKNOWLEDGMENT

This work was supported by a research grant to JB from the Canadian Natural Sciences and Engineering Research Council.

REFERENCES

1. A. Durif-Varambon, *Bull. Soc. Fr. Miner. Cristallogr.* **82,** 285 (1959).
2. J. Barbier, *Eur. J. Solid State Inorg. Chem.* **31,** 163 (1994).
3. K. Hartl and R. Braumgart, *Z. für Naturforsch. B* **33,** 954 (1978).
4. J. M. Visser, *J. Appl. Crystallogr.* **2,** 89 (1969).
5. D. M. C. Guimaraes, *Acta Crystallogr. Sect. A* **35,** 108 (1979).
6. A. Sakthivel and R. A. Young, "DBWS-9006PC Rietveld Analysis Package," Georgia Institute of Technology, Atlanta, 1992.
7. J. Barbier, J. E. Greedan, T. Asaro, and G. J. McCarthy, *Eur. J. Solid State Inorg. Chem.* **27,** 855 (1990).
8. J. Barbier, *J. Solid State Chem.* **101,** 249 (1992).
9. M. O'Keeffe and S. Andersson, *Acta Crystallogr. Sect. A* **33,** 914 (1977).
10. R. D. Shannon, *Acta Crystallogr. Sect. A* **32,** 751 (1976).
11. I. D. Brown and D. Altermatt, *Acta Crystallogr. Sect. B* **41,** 244 (1985).
12. H. N. Ng and C. Calvo, *Can. J. Phys.* **53,** 42 (1975).
13. K. Sugiyama and M. Tokonami, *Mineral. J.* **15,** 141 (1990).
14. J. M. Kiat, P. Garnier, and M. Pinot, *J. Solid State Chem.* **91,** 339 (1991).
15. W. Carrillo-Cabrera and H. G. von Schnering, *Z. Kristallogr.* **205,** 271 (1993).
16. G. J. McCarthy and D. E. Pfoertsch, *J. Solid State Chem.* **38,** 128 (1981).